# IMPORTANCE OF OVERLAND FLOW IN DENITRIFICATION OF WASTEWATER APPLIED TO RAPID INFILTRATION BASINS

Maryam Akhavan[1], Paul T. Imhoff[1], Scott Andres[2], Stefan Finsterle[3]

[1]Department of Civil and Environmental Engineering, University of Delaware
Newark, DE 19716, USA
e-mail: makhavan@udel.edu

[1] Delaware Geological Survey
Newark, DE 19716, USA

[3]Earth Sciences Division, Lawrence Berkeley National Laboratory
Berkeley, CA 94720, USA

## ABSTRACT

Rapid Infiltration Basin Systems use the controlled application of treated wastewater to soil to remove constituents in the wastewater before recharging groundwater. Effluent from most new wastewater treatment plants is enriched in $NO_3^-$, so denitrification (DNF) is the main reaction for N removal. The absence of molecular oxygen and an adequate supply of carbon to serve as a substrate for heterotrophic bacteria are the required conditions for DNF.

During RIBS operation, wastewater is applied to open basins cyclically, usually with a flooding period followed by days or weeks of drying. Key operational parameters impacting DNF include the ratio of wetting to drying time and the hydraulic loading rate, which affect water saturation and air content in the vadose zone and residence time of contaminants. To investigate the effects of complex surface and subsurface flow patterns caused by non-uniform flooding on system performance, we applied a coupled overland flow-vadose zone model previously implemented in iTOUGH2 to TOUGHREACT. The flow portion of the coupled code was previously tested with published laboratory and field data. This modified TOUGHREACT was then used to investigate effects of operating conditions on the fate and transport of N.

Simulations with the coupled overland flow-vadose zone model predict uneven water distribution over the basins, a condition that significantly affects DNF. Smaller ratios of wetting to drying time, i.e., shorter but more intense flooding periods, result in greater water saturations, shorter residence times, and lower oxygen concentrations in the vadose zone, ultimately resulting in greater DNF. For the same reasons, higher loading rates also result in greater DNF, because of favored growth of microbial communities at deeper depths. Using a coupled surface-subsurface model is critical for predicting DNF when the hydraulic loading rate is not sufficiently large to quickly spread the wastewater over the whole basin.

## INTRODUCTION

Rapid infiltration basin systems (RIBS) are one of the major land-treatment techniques for disposal and treatment of reclaimed wastewater (US EPA, Office of Water, 2003). In these systems, treated wastewater using primary, secondary, or advanced treatment techniques is disposed into shallow basins constructed in permeable soils such as sand. Effluents from wastewater treatment systems potentially contain a number of contaminants, and nitrogen (N) compounds are of particular concern.

During RIBS operations, wastewater is applied intermittently in a cycle of a flooding period–wastewater application—followed by days or weeks of drying (NRMRL, 2006; US EPA, 1984). The drying period is required for restoration of the infiltration capacity and allows renewal of the biological and chemical treatment capability of the soil. As a result, the ratio of flooding to drying time (referred to here as the application cycle) is critical to the successful operation of RIBS and varies with the quality of

applied wastewater and soil type. This ratio is recommended to be between 0.5 to 1.0 when N removal is the main objective of RIBS operations and the wastewater is not completely nitrified (NRMRL, 2006; US EPA, 1984). In this case, the effluent must first be nitrified and then denitrified. Therefore, oxic conditions in the vadose zone are required for nitrification. However, in most new sequenced batch reactor wastewater treatment plants, a fully nitrified wastewater is applied and DNF is the primary reaction for removing N from subsurface water. In this case, anoxic conditions and an adequate supply of organic C are critical for DNF. There are no EPA recommendations for the ratio of flooding to drying time for such systems.

Another design parameter is the hydraulic loading rate within each application cycle, which affects $O_2$ availability, pore-water velocity, and thus retention time. Because of the fixed total amount of wastewater discharged on a basin, the loading rate and application cycle are interdependent. For example, achieving a low loading rate may require a high ratio of flooding to drying time.

In previous modeling and experimental studies of RIBS, the basin was always assumed to be flooded completely and instantaneously during the flooding period (Gungor and Kahraman, 2005; Kopchynski et al., 1996). However, the use of a low applied loading rate and overdesign of the required infiltration area in many RIBS will cause nonhomogeneous distribution of wastewater (Mottier et al., 2000), and the conditions under which water reaches areas farthest from the discharge valves by overland flow after the infiltration capacity of areas nearest discharge valves is exceeded.

The objective of this work was to apply a coupled surface–subsurface flow model in TOUGHREACT to elucidate the utility of existing approaches for estimating DNF under RIBS when wastewater is applied non-uniformly due to overland flow, and to study effects of operating conditions and wastewater quality on N fate and transport. The flow portion of the coupled code was previously tested with published laboratory and field data (Akhavan et al., 2012).

## MODEL DEVELOPMENT

Numerical simulations were performed using TOUGHREACT v1.1 (Xu et al., 2006; Xu, 2008). Modifications previously implemented in iTOUGH2 that coupled overland flow with subsurface transport were added to TOUGHREACT v1.1, and the flow portion of the coupled code was retested.

### Surface and Subsurface Flow Equations

The Saint-Venant equations were used to model surface-water flow, where the diffusion wave (non-inertial wave) form was chosen for the momentum equation. The surface-water flow equations were coupled with the two-phase flow equations for water and air (EOS3). A surface layer of thickness $e$ was assumed superimposed on the topsoil layer in the numerical model. Liquid flow within the surface layer was presented in a similar form that describes flow in a porous medium:

$$\frac{\partial h_s}{\partial t} - \nabla \cdot \left( K_s \nabla (z_l + h_s) \right) = q_s$$

where $h_s$ is the water depth on the surface [L], $K_s$ is the hydraulic conductivity tensor [$LT^{-1}$], $z_l$ is land surface elevation [L], and $q_s$ is a source/sink term [$LT^{-1}$]. The nondiagonal terms of the hydraulic conductivity tensor $K_s$ are zero and the diagonal components are

$$K_{s,xx} = \frac{h_s^{5/3}}{n_{man} \sqrt{\nabla_x (z_l + h_s)}}$$

$$K_{s,yy} = \frac{h_s^{5/3}}{n_{man} \sqrt{\nabla_y (z_l + h_s)}}$$

$$K_{s,zz} = k_{zz} \frac{k_{rl}}{\mu_l}$$

The horizontal hydraulic conductivities describe surface water flow, while the vertical hydraulic conductivity describes resistance to liquid flow between the surface and subsurface layer, with $k_{zz}$ equal to the vertical permeability of the subsurface layer, and $n_{man}$ the Manning roughness coefficient [$L^{-1/3}T$]. More details of the coupling approach are given in Akhavan et al. (2012).

## Solute Transport and Biogeochemical Reactions

The macroscopic equations governing aqueous and gaseous advective–diffusive transport in a variably saturated porous medium were used for solving transport of chemical species. The multiple Monod expression was used for describing kinetic reactions among primary species (Xu, 2008)

$$r_i = \hat{k}_i X_m F(X_m)\left[\frac{C_{i,k}}{C_{i,k} + \hat{K}_{Mi,k}}\right]\left[\frac{\hat{K}_{i,p}}{C_{i,p} + \hat{K}_{i,p}}\right] f(pH)$$

where $r_i$ is the reaction rate of the $i$th reaction, $\hat{k}_i$ is the maximum specific consumption rate, $X_m$ is the biomass of the population $m$ responsible for the reaction, $F(X_m)$ is the biomass growth inhibition term (MacQuarrie and Sudicky, 2001), $C_{i,k}$ is the concentration of the $k$th Monod species, $C_{i,p}$ is the concentration of the $p$th inhibiting factors, $\hat{K}_{Mi,k}$ and $\hat{K}_{i,p}$ are the $k$th Monod half-saturation constant of the $i$th species and the $p$th inhibition constant, and $f(pH)$ is the piecewise linear function accounting for microbial acidity stress (Maggi et al., 2008):

$$f(pH) = \begin{cases} \min\left[\frac{1}{4}pH - \frac{3}{4}, -\frac{1}{4}pH + \frac{11}{4}\right] & 3 < pH < 11 \\ 0 & Otherwise \end{cases}$$

In order to account for rate limitations as a result of excessive biomass accumulation, a biomass growth inhibition term was incorporated in the Monod expression (Kindred and Celia, 1989)

$$F(X_m) = \frac{\hat{K}_{b,m}}{\hat{K}_{b,m} + X_m}$$

where $\hat{K}_{b,m}$ is an empirical inhibition constant. As discussed by Kindred and Celia (1989), when the biomass of the population $m$ becomes much larger than $\hat{K}_{b,m}$, the reaction rate formula is similar to the basic Michaelis-Menton expression except that the biomass is replaced by the constant $\hat{K}_{b,m}$. The effect of microbial volume augmentation on soil porosity and its effect on water flow were neglected.

### *Biodegradation reactions*

The carbon oxidation and DNF reactions were

$$CH_2O + O_2 \xrightarrow{X_1} CO_2 + H_2O$$

$$CH_2O + \frac{4}{5}NO_3^- \xrightarrow{X_1} \frac{2}{5}N_2 + \frac{2}{5}H_2O + \frac{1}{5}H^+ + HCO_3^-$$

and were modeled using the multiple Monod expression. It was assumed that the same bacteria population, $X_1$, was responsible for both reactions. Production of intermediate N compounds such as NO and $N_2O$ were not included in the formulation because the focus of this study was on $NO_3$ removal. A kinetic dissolution model presented by Jardine et al. (1992) was used for modeling adsorption and dissolution of dissolved organic carbon

$$\frac{d\,\overline{DOC}}{dt} = \alpha_d (K_d \times DOC - \overline{DOC})$$

where $DOC$ is the dissolved organic carbon concentration [$ML^{-1}$], $\overline{DOC}$ is the mass of solid organic carbon per mass of solid [$MM^{-1}$], $\alpha_d$ is a first-order mass-transfer coefficient [$T^{-1}$], and $K_d$ is a linear distribution coefficient [$L^3M^{-1}$]. $K_d$=50 L $kg^{-1}$ and $\alpha_d = 4.21\times10^{-7}\,S^{-1}$ were used for these simulations. Monod parameters are given in Table 1.

*Table 1. Monod parameters used for simulations*

| Parameter | Value |
|---|---|
| Death rate of bacteria ($d^{-1}$) | 0.05 |
| Max. carbon oxidation rate ($d^{-1}$) | 4.9 |
| Max. DNF rate ($d^{-1}$) | 4.9 |
| Half saturation constant $NO_3$ (mg $L^{-1}$) | 0.5 |
| Half saturation constant *DOC* (mg $L^{-1}$) | 7.41 |
| Half saturation constant $O_2$ (mg $L^{-1}$) | 0.2 |
| $O_2$ Inhibition constant (mg $L^{-1}$) | 0.2 |
| Microbial yield coefficient (-) | 0.63 |

## RAPID INFILTRATION BASIN SIMULATIONS

To study the effects of a spatially non-uniform distribution of wastewater, hydraulic loading rate, and application cycle on DNF in RIBS, we simulated different scenarios using the coupled surface–subsurface code that accounts for overland flow. Initial and boundary conditions and other RIBS properties were selected to represent a common scenario in RIBS operation.

A number of simulations were conducted with a specified flux boundary at the basin surface to reproduce the approach used in conventional modeling studies.

We developed a two-dimensional, vertical model 55.5 m long and 26.1 m in depth, which represented one-half of the physical domain. The horizontal grid size ranged from 0.05 to 1 m, with a refined grid beneath the basin area, and the vertical grid size ranged from 0.02 to 1 m, with a refined grid in the unsaturated zone. The infiltration basin in the model was 5 m wide and positioned at the top left-hand boundary, with wastewater distribution represented as a line source on the left edge of the basin. This line source represented a distribution pipe. A schematic of the model domain is shown in Figure 1. The thickness of the surface layer for overland flow was defined as 1 m.

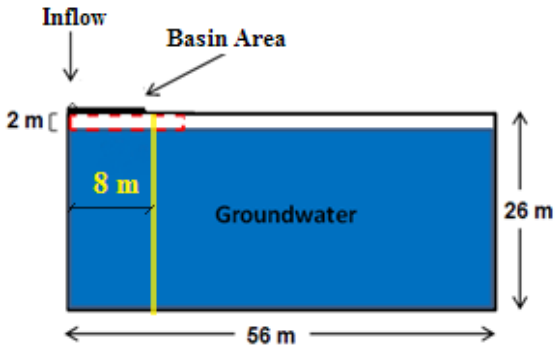


Figure 1. Schematic of model domain. The denitrification reduction factor, $F_s$, was calculated in the dashed red rectangle. Vertical yellow line is the compliance boundary where $NO_3$ concentrations were monitored in groundwater.

Sand—USDA textural class—was used for simulations, and the ROSETTA pedotransfer function model was used to estimate the parameters of the van Genuchten–Mualem model for this soil, using the textural class option (Radcliffe and West, 2009) (Table 2). A homogeneous medium with an anisotropy ratio of $k_{xx}/k_{zz} = 10$ was assumed for all simulations.

*Table 2. Hydraulic parameters used for modeling*

| $K_{s,z}$ (cm d$^{-1}$) | n | $\alpha$ (cm$^{-1}$) | $\theta_r$ | $\theta_s$ |
|---|---|---|---|---|
| 645 | 3.18 | 0.0353 | 0.053 | 0.375 |

Initial conditions were defined by an equilibrium head distribution, with the water table located at a depth of 2.05 m below the basin floor. No-flow boundary conditions were defined for the bottom and left boundary of the model, while at the right boundary, a constant-head boundary condition was specified, sufficiently far from the basin to minimize its effect on simulation results. Initial conditions and wastewater source properties for selected aqueous species are listed in Table 3. The RIBS were simulated with three alternative hydraulic loading rates and two application cycles. The three hydraulic loading rates were 0.5, 0.75, and 1 m wk$^{-1}$ (L2–L4), while the application cycle was either 0.5 flooding days followed by 6.5 drying days (C1), or three flooding days followed by four drying days (C2). The total amount of wastewater discharged in the basin in each 7 d cycle was identical for a particular hydraulic loading rate. The three hydraulic loading rates tested are equivalent to annual loading rates of 13 to 52 m yr$^{-1}$.

*Table 3. Initial conditions and wastewater source properties for selected aqueous species*

| Aqueous species | Initial Value | Source Value |
|---|---|---|
| $NO_3$ (mole L$^{-1}$-$N$) | 0.0 | 10.0 |
| $DOC$ (mg L$^{-1}$) | 0.0 | 25.0 |
| $\overline{DOC}$ (mg mg$^{-1}$) | 0.0 | 0.0 |
| $O_2$* (mole L$^{-1}$) | 0-8m: $2.3\times10^{-4}$<br>8-10m: $1.3\times10^{-4}$<br>10-26m: $3\times10^{-5}$ | $2.3\times10^{-4}$ |
| $pH$ | 6.9 | 6.0 |
| $HCO_3$ (mole L$^{-1}$) | $1.7\times10^{-5}$ | $3.9\times10^{-5}$ |
| $N_2$ (mole L$^{-1}$) | 0.0 | 0.0 |
| $X_1$ (mg L$^{-1}$) | 0.47 | 0.0 |

*$O_2$ is given in different depths.

Simulations were run for 8 weeks until quasi-steady-state conditions were achieved, where the change in percent removal of $NO_3$ and $DOC$ (described below) between consecutive cycles was <2%. The right boundary was specified sufficiently far enough from the discharge valve that the wastewater plume did not reach this boundary in 8 weeks.

The results of the three hydraulic loading rates and two application cycles were compared using two performance measures. The first was the percent removal of $NO_3$ and *DOC*, which was computed by subtracting the current $NO_3$ (*DOC*) in the domain from the total added $NO_3$ (*DOC*), normalized by the total mass added. The second performance measure was the maximum $NO_3$ concentration in a vertical cross section (compliance plane) located 8 m from the discharge valve (see Figure 1).

The effect of operating conditions on DNF was also studied using a simplified approach that accounts for the impact of pore water saturation on DNF. In this approach, a variable, $F_s$, was introduced, which is a measure of the reduction in DNF because liquid saturation conditions were not ideal. Liquid saturation is an important parameter that controls $O_2$ diffusion from the atmosphere and affects local $O_2$ concentrations in pore water. Anoxic conditions are one requirement for DNF, but modeling $O_2$ dynamics in the subsurface is complicated. Therefore, liquid saturation was used as a surrogate variable to evaluate $O_2$ limitations in the pore water in previous work (Heinen, 2006; Vereecken et al., 1991). $F_s$, the reduction factor due to water saturation, was defined as

$$F_s = \begin{cases} 0 & S_l < S_t \\ \left( \dfrac{S_l - S_t}{S_m - S_t} \right)^w & S_t \le S_l \le S_m \\ 1 & S_m < S_l \end{cases}$$

where $S_l$ is liquid saturation, $S_m$ is a threshold liquid saturation above which $F_s = 1$, and $S_t$ is a value below which $F_s = 0$. We selected $S_m = 1$, $S_t = 0.62$, and $w = 1.74$. In our simulations, $F_s$ was computed in a rectangular region beneath the infiltration basin, as shown in Figure 1. It was evaluated at each location in the rectangular region and then averaged across space. More details are presented in Akhavan et al. (2012).

Two values for $\hat{K}_{b,m}$ were tested: 1 and 10 $mgL^{-1}$. These values were selected such that biomass growth did not reduce initial porosity more than 20%, and as a result would not significantly affect hydraulic conductivity. The fraction of pore space occupied by biomass, $n_{X'_m}$, was estimated from Brovelli et al. (2009); Kildsgaard and Engesgaard (2001); and Lee et al., (2009):

$$n_{X'_m} = \frac{X'_m \rho_b}{\rho_{X'_m}}$$

where $\rho_b$ is the bulk density [$ML^{-3}$], $\rho_{X'_m}$ is the density of solid biomass [$ML^{-3}$], and $X'_m$ is solid biomass concentration [$MM^{-1}$]. $\rho_{X'_m}$ was considered to be in the range of 2500–6000 $mgL^{-1}$ (Kildsgaard and Engesgaard, 2001). Using $\hat{K}_{b,1}$=1 and 10 $mgL^{-1}$ limited maximum biomass concentration to less than 600 $mgL^{-1}$. $\hat{K}_{b,1}$= 0.5 and 1 $mgL^{-1}$ were used in previous numerical studies (Lee et al., 2006; MacQuarrie and Sudicky, 2001)

## MODELNG RESULTS

### Removal Process

To illustrate $NO_3$ removal and system dynamics, we present results after 8 weeks of wastewater flooding. Figure 2 shows water saturation, $NO_3$, biomass, and $O_2$ (aq) biomass contours for loading rate 4, application cycle 1 (L4C1), and loading rate 4, application cycle 2 (L4C2) after flooding in week 8. $\hat{K}_{b,1}$=1 mg $L^{-1}$ was used in these two simulations. Contours are shown for a 30 m wide and 15 m deep portion of the domain beneath the basin. Because of the higher instantaneous hydraulic loading rate in cycle 1 versus cycle 2 (loading over 0.5 versus 3 days), the area below the RIBS has higher water saturation for L4C1. However, $NO_3$ contours indicate that in both application cycles, DNF occurs primarily beneath the water table. $O_2$ contours show that although soil under the basin is more saturated for L4C1 than L4C2, an anoxic zone in both cycles only forms beneath the water table.

Because of the lower instantaneous hydraulic loading rate in L4C2 than L4C1, higher biomass concentrations developed for L4C2 in the vadose zone beneath the basin (see Figure 2). For example, the maximum biomass concentration in this region was 66 and 41 mg $L^{-1}$ for L4C2 and L4C1, respectively. Although the total biomass produced for L4C2 and L4C2 was nearly the same, the higher loading rate for L4C1 resulted in lower biomass growth under

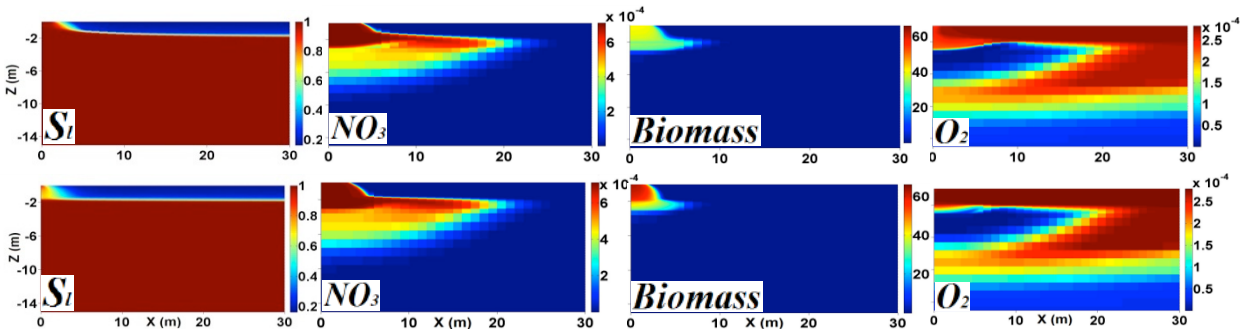


Figure 2. Water saturation, $S_l$ (-); $NO_3$(mole $L^{-1}$); biomass(mg $L^{-1}$); and $O_2$(aq) (mole $L^{-1}$) contours for L4C1 (top) and L4C2 (bottom)

the basin but a more extensive region of biological growth laterally, due to the greater lateral movement of water and substrate. Thus, shorter but more intense flooding periods distribute biomass over a larger area, and in some cases to greater depths (e.g., for $\hat{K}_{b,1}$=10 mg $L^{-1}$ simulations not shown here), which could improve DNF when the biomass growth is extended to the anoxic zone under the water table.

The first moment of biomass and *DOC* were computed in the Z direction in a 5 m long and 6 m deep region beneath the infiltration basin after flooding in week 8. The total mass of *DOC* was also computed in this region. These results for $\hat{K}_{b,1}$=1 mg $L^{-1}$ are shown in Figure 3.

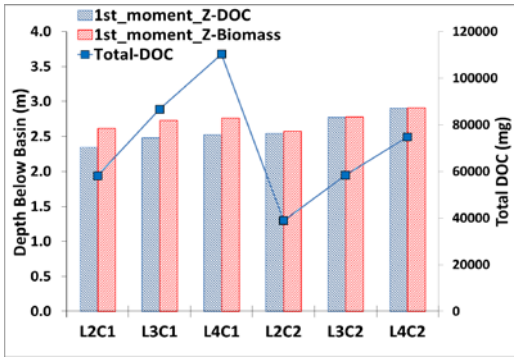


Figure 3. First moment and total mass of *DOC* beneath the basin for $\hat{K}_{b,1}$= 1 mg $L^{-1}$ for different loading rates and application cycles.

As the hydraulic loading rate increased from L2 to L4 (0.5 to 1.0 m per week) for both cycles (C1 and C2), the residence time in the vadose zone decreased, and more substrate (*DOC*) and biomass were transmitted downward, resulting in larger first moments. The results are similar for $\hat{K}_{b,1}$=10 mg $L^{-1}$. As will be shown below, application of larger loading rates improves DNF, because it develops biomass at greater depths and preserves more carbon for DNF under the water table (see the first moment of biomass and total *DOC* plotted in Figure 3). For the same loading rates, application of shorter flooding periods (cycle 1 versus cycle 2) improves DNF as well, because the residence time of *DOC* in the vadose zone is reduced, resulting in less *DOC* oxidation. For these cases, more of the *DOC* is transported below the water table where it supports DNF.

To evaluate where DNF occurred, concentrations of $NO_3$ and a conservative tracer with the same loading as $NO_3$ were examined at different depths to compute the cumulative percent $NO_3$ removal at the end of the flooding period in week 8. Figure 4 shows cumulative $NO_3$ removal versus depth for $\hat{K}_{b,1}$=1 mg $L^{-1}$.

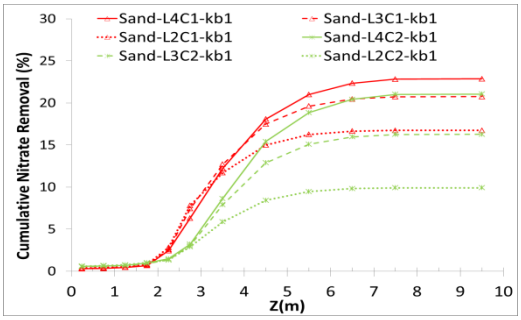


Figure 4. Cumulative $NO_3$ percent removal over depth

DNF occurred almost entirely beneath the water table at depths of 2–7 m for both cycles. In both

cycles, cumulative DNF was larger for higher loading rates, ranging from 16 to 23% for cycle 1 and from 10 to 21% for cycle 2. The DNF zone extended to greater depths as loading rate increased. For the same loading rate, DNF was also larger in cycle 1 (shorter flooding period), than cycle 2, where the higher DNF occurred at the depth of 2–3 m.

While results presented above were for $\hat{K}_{b,1}$=1 mg $L^{-1}$, similar trends and conclusions regarding the impact of hydraulic loading rate and application cycle on DNF were drawn from simulations with $\hat{K}_{b,1}$=10 mg $L^{-1}$.

## Microbial Growth Model vs. Simplified Process Model

Figure 5 shows $NO_3$ removal for alternative loading rates and application cycles predicted with the microbial growth model and the simplified process model, where an average $NO_3$ reduction factor was calculated ($F_s$). Water saturations used in the calculation of $F_s$ and shown in this figure were averaged over a 5 m long and 2 m deep region beneath the infiltration basin. The simplified process model evaluates DNF by only accounting for water saturation and predicts much larger DNF than the microbial growth model. However, the simplified process model and microbial growth model both show increasing DNF with loading rate for a given cycle, and higher DNF for cycle 1 than cycle 2. The final cumulative $NO_3$ removed shown in Figure 4 for the vertical region beneath the basin were in good agreement with $NO_3$ removal computed for the entire domain in Figure 5.

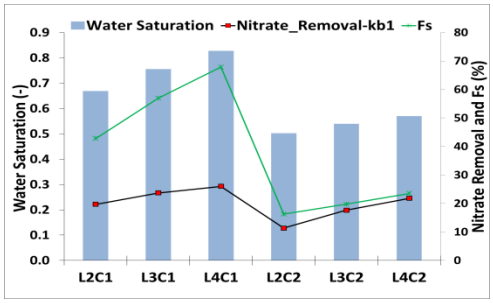


Figure 5. $NO_3$ removal for alternative loading rates and application cycles computed with the microbial growth model and $F_s$ from the simplified process model

To evaluate the effect of different operating conditions on reducing $NO_3$ concentrations in the groundwater, $NO_3$ concentrations were computed in a vertical cross section located 8 m from the discharge valve (see Figure 1). Although percent $NO_3$ removed increased by applying higher loading rates and using shorter but more intense flooding periods (see Figure 5), the maximum $NO_3$ concentration along the compliance boundary did not differ significantly for alternative operating conditions: the maximum $NO_3$ concentration was reduced by 1.7–4.5% from that in the discharged wastewater, which is negligible.

The primary limitation on DNF was the lack of sufficient *DOC* in the effluent for $NO_3$ removal. In a well well-mixed system and assuming no *DOC* is consumed by the carbon oxidation reaction, 10.7 $mgL^{-1}$ *DOC* is required for DNF of 10 $mgL^{-1}$ $NO_3$. However, because of oxic conditions in the vadose zone, even the 25 $mgL^{-1}$ *DOC* applied here was insufficient for complete DNF of the 10 $mgL^{-1}$ $NO_3$. Instead, DNF ranged from 11 to 26%, depending on operating conditions (see Figure 5).

## Overland Flow Top Boundary Condition vs. Specified Flux

For the simulations where a specified flux was assumed across the top boundary, the same loading rates used in the overland flow simulations were applied, except that each loading rate was spread evenly across the total basin area. Figure 6 shows $NO_3$ removal predicted with the overland flow boundary was higher than removal predicted using a specified flux boundary condition for both $\hat{K}_{b,1}$. Thus, the error in neglecting overland flow on $NO_3$ removal is significant and can exceed 300%.

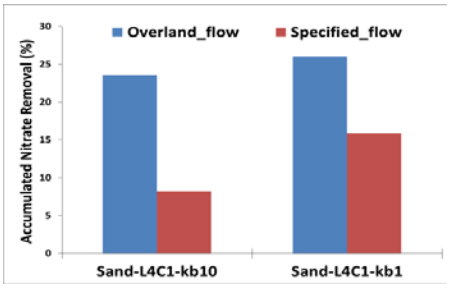


Figure 6. $NO_3$ removal using overland flow and specified flux boundary conditions

## CONCLUSIONS

Rapid infiltration basin-system operations are guided by requirements to reduce $NO_3$ to maximum acceptable groundwater concentrations. Anoxic conditions and an adequate supply of carbon are required for DNF. In the absence of other electron donors, carbon is consumed by microbial oxidation. Percent $NO_3$ removed was found to be sensitive to the basin boundary condition—either overland flow or a specified flux boundary—the hydraulic loading rate, and the flooding/drying period ratio. However, because of insufficient *DOC*, maximum $NO_3$ removal was <30% for all operating conditions. The most significant DNF occurred for high loading rates and small flooding/drying ratios. Here, the residence time of *DOC* in the vadose zone was reduced, allowing more to reach the anoxic zone under the water table where it was available for DNF.

In this study, the commonly assumed specified flux boundary condition resulted in underpredictions of DNF by as much as 300%.

## ACKNOWLEDGMENTS

The authors thank Dr. Chuanhui Gu and Dr. Federico Maggi for their help with TOUGHREACT. Financial support for this study was provided by the Delaware Water Resources Center.

## REFERENCES

Akhavan M., Imhoff P.T., Finsterle S. and Andres A.S. 2012. Application of a coupled overland Flow–Vadose zone model to rapid infiltration basin systems. Vadose Zone Journal 11.

Brovelli A., Malaguerra F. and Barry D.A. 2009. Bioclogging in porous media: Model development and sensitivity to initial conditions. Environmental Modelling & Software 24:611-626.

Gungor K. and Kahraman U. 2005. Nitrite and nitrate removal efficiencies of soil aquifer treatment. Turkish J.Eng.Env.Sci 29:159-170.

Heinen M. 2006. Simplified denitrification models: Overview and properties. Geoderma 133:444-463.

Jardine P.M., Dunnivant F.M., Selim H.M. and Mccarthy J.F. 1992. Comparison of models for describing the transport of dissolved organic-carbon in aquifer columns. Soil Sci. Soc. Am. J. 56:393-401.

Kildsgaard J. and Engesgaard P. 2001. Numerical analysis of biological clogging in two-dimensional sand box experiments. J. Contam. Hydrol. 50:261-285.

Kindred J.S. and Celia M.A. 1989. Contaminant transport and biodegradation .2. conceptual-model and test simulations. Water Resour. Res. 25:1149-1159.

Kopchynski T., Fox P., Alsmadi B. and Berner M. 1996. The effects of soil type and effluent pre-treatment on soil aquifer treatment. Water Sci. Technol. 34:235-242.

Lee E.J., Kim M., Kim Y. and Lee K. 2009. Numerical and field investigation of enhanced in situ denitrification in a shallow-zone well-to-well recirculation system. Ecol. Model. 220:2441-2449.

Lee M.S., Lee K.K., Hyun Y.J., Clement T.P. and Hamilton D. 2006. Nitrogen transformation and transport modeling in groundwater aquifers. Ecol. Model. 192:143-159.

MacQuarrie K.T.B. and Sudicky E.A. 2001. Multicomponent simulation of wastewater-derived nitrogen and carbon in shallow unconfined aquifers I. model formulation and performance. J. Contam. Hydrol. 47:53-84.

Maggi F., Gu C., Riley W.J., Hornberger G.M., Venterea R.T., Xu T., Spycher N., Steefel C., Miller N.L. and Oldenburg C.M. 2008. A mechanistic treatment of the dominant soil nitrogen cycling processes: Model development, testing, and application. Journal of Geophysical Research-Biogeosciences 113:G02016.

Mottier V., Brissaud F., Nieto P. and Alamy Z. 2000. Wastewater treatment by infiltration percolation: A case study. Water Sci. Technol. 41:77-84.

NRMRL. 2006. Process design manual; land treatment of municipal wastewater effluents. U.S. Environmental Protection Agency, National Risk Management Research Laboratory, Office of Research and Development, Land Remediation and Pollution Control Division, Cincinnati, OH.

Radcliffe D.E. and West L.T. 2009. Design hydraulic loading rates for onsite wastewater systems. Vadose Zone J. 8:64-74.

US EPA. 1984. Process design manual for land treatment of municipal wastewater, supplement on rapid infiltration and over-land flow. Rep. EPA 625/1-81-013a. U.S. Environmental Protection Agency, Cincinnati, OH.

US EPA, Office of Water. 2003. Wastewater technology fact sheet: Rapid infiltration land treatment. Rep. EPA 832-F-03-025.

Vereecken H., Vanclooster M., Swert M. and Diels J. 1991. Simulating water and nitrogen behavior in soils cropped with winter-wheat. Fertilizer Research 27:233-243.

Xu T.F., Sonnenthal E., Spycher N. and Pruess K. 2006. TOUGHREACT - A simulation program for non-isothermal multiphase reactive geochemical transport in variably saturated geologic media: Applications to geothermal injectivity and CO2 geological sequestration. Comput. Geosci. 32:145-165.

Xu T. 2008. Incorporating aqueous reaction kinetics and biodegradation into TOUGHREACT: Applying a multiregion model to hydrobiogeochemical transport of denitrification and sulfate reduction. Vadose Zone Journal 7:305-315.